CMS Physics Analysis Summary

Contact: cms-pag-conveners-susy@cern.ch 2013/05/29

Search for supersymmetry in pp collisions at $\sqrt{s} = 8$ TeV in events with three leptons and at least one b-tagged jet

The CMS Collaboration

Abstract

Results are reported from a search for new physics processes in events with three leptons and at least one b-tagged jet. The analysis is based on a sample of proton-proton collisions at a center-of-mass energy of 8 TeV with an integrated luminosity of 19.5/fb, collected by the CMS detector at the LHC. The event selection focuses on signatures for supersymmetry (SUSY) that include multiple W or Z bosons and b-jets in the final state, and the b-jet multiplicity is used to define low-background search regions. The standard model background contributions are determined using well-established techniques that are based on control samples in the data. The observed yields in the data are consistent with the background predictions, and the results are used to obtain upper limits on the production cross sections for several SUSY event topologies defined in the framework of simplified models.

1 Introduction

A broad range of searches for supersymmetry (SUSY) [1–7] and other new physics (NP) has been performed by the CMS and ATLAS experiments [8]. These include generic searches for signatures with jets, missing transverse energy ($E_{\mathrm{T}}^{\mathrm{miss}}$), and leptons. Multilepton searches [9–12] have played an important role, partly because the presence of multiple leptons strongly suppresses backgrounds, allowing other selection requirements, such as $E_{\mathrm{T}}^{\mathrm{miss}}$, to be relaxed.

For SUSY models that predict the production of third generation scalar quarks (squarks), the addition of a b-jet requirement in the signature provides a powerful tool that has been exploited in several searches [9–11]. SUSY scenarios leading to the production of light stop ($\widetilde{\mathrm{t}}_1$), sbottom ($\widetilde{\mathrm{b}}_1$), and gluino ($\widetilde{\mathrm{g}}$) are well motivated theoretically [13–15] and have only been partially explored by existing searches. The motivation arises from naturalness considerations related to protecting the Higgs mass against large loop corrections in the standard model (SM) [13, 16, 17]. The first- and second-generation squarks, in contrast, are not required to be light in such scenarios.

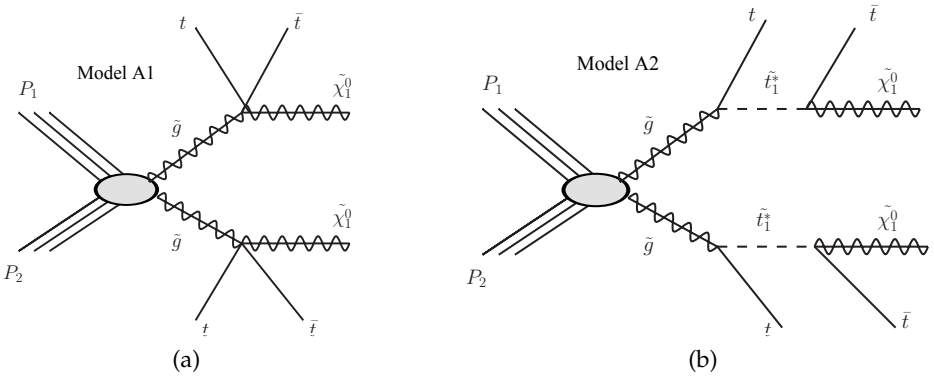

Figure 1: Processes targeted by this analysis include $\widetilde{\mathrm{g}}$-pair production with subsequent decay to four top quarks and two lightest SUSY particles (LSP) ($\mathrm{pp} \to \widetilde{\mathrm{g}}\widetilde{\mathrm{g}} \to \mathrm{t\bar{t}t\bar{t}}\widetilde{\chi}_1^0\widetilde{\chi}_1^0$) via (a) off-shell and (b) on-shell top squark.

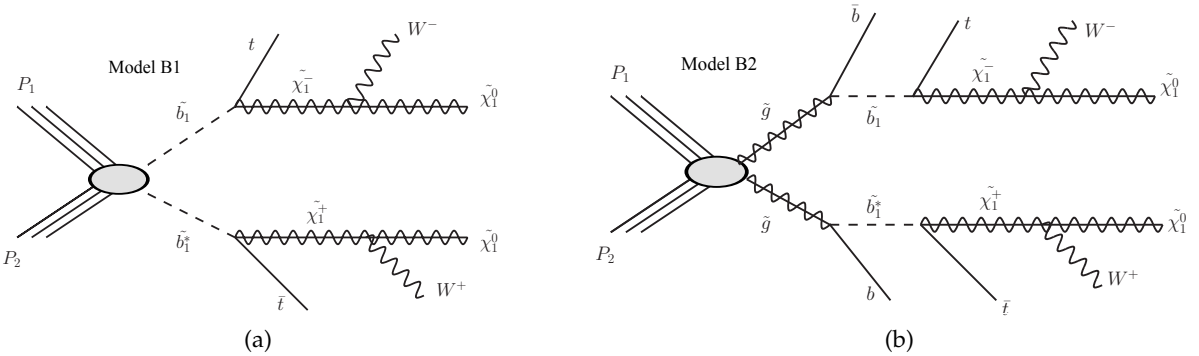

Figure 2: Processes targeted by this analysis include (a) direct $\widetilde{\mathrm{b}}_1$-pair production with decay to two top quarks, two W and two LSP ($\mathrm{pp} \to \widetilde{\mathrm{b}}_1\widetilde{\mathrm{b}}_1^* \to \mathrm{t\bar{t}WW}\widetilde{\chi}_1^0\widetilde{\chi}_1^0$), and (b) $\widetilde{\mathrm{g}}$-pair production with decay to two bottom quarks, two top quarks, two W bosons, and two LSP via on-shell bottom squark ($\mathrm{pp} \to \widetilde{\mathrm{g}}\widetilde{\mathrm{g}} \to \mathrm{b\bar{b}t\bar{t}WW}\widetilde{\chi}_1^0\widetilde{\chi}_1^0$).

Figure 1 shows an example of one such scenario: the production of a pair of gluinos ($\tilde{g}$), which decay to four top quarks and two neutralinos. The gluino decays via $\tilde{g} \to \tilde{t}_1 t$, where the $\tilde{t}_1$ can be either virtual (Fig. 1a) or real (Fig. 1b). The corresponding experimental signature has four b-jets, four W bosons (decaying either into leptons or jets), and substantial E_T^{miss}. A second example, shown in Fig. 2, is a direct production of $\tilde{b}_1$-squarks (Fig. 2a) or a production of gluinos which decay to a bottom anti-quark and a bottom squark (Fig. 2b). In these two models, $\tilde{b}_1$-squarks decay into a top quark and a chargino which then yields the W boson and the LSP. Here, the experimental signature includes two b-jets, four W bosons, and large E_T^{miss}.

The scenario with Z bosons and b-jets in the final state can be realized in case of the sbottom-pair production where each $\tilde{b}_1$ decays to a b-quark and a heavy neutralino, e.g. $\tilde{\chi}_2^0$. In turn, the latter yields a Z boson and the lightest neutralino $\tilde{\chi}_1^0$ (Fig. 3). In SUSY, this event topology has a significant branching fraction, e.g. when the sbottom is mostly right-handed and $\tilde{\chi}_2^0$ ($\tilde{\chi}_1^0$) is mostly higgsino-like (wino-like).

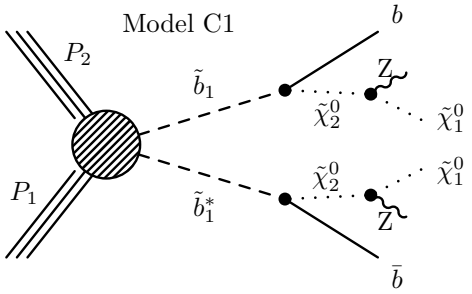

Figure 3: Process targeted by this analysis includes direct $\tilde{b}_1$-pair production with decay to two b-quarks, two Z and two LSP ($pp \to \tilde{b}_1\tilde{b}_1^* \to b\bar{b}ZZ\tilde{\chi}_1^0\tilde{\chi}_1^0$).

This search is sensitive to the production of light stop and sbottom in decay final states that include at least three isolated light leptons (e or μ), b-tagged jets, E_T^{miss}, and a substantial amount of hadronic activity in the form of energetic jets. We use a dataset collected with the Compact Muon Solenoid (CMS) detector [18] in 2012 corresponding to 19.5 $fb^{-1}$of integrated luminosity of proton-proton (pp) collisions at a center-of-mass energy of 8 TeV.

Compared to single lepton or like-sign dilepton signatures, a trilepton search targets final states that are produced with lower branching fractions but nevertheless provides good signal sensitivity because the three-lepton signature strongly suppresses backgrounds. Only a handful of SM processes have such a signature. The most prominent SM background in trilepton final states is WZ production. In this analysis, this background is highly suppressed by requiring at least one b-tagged jet.

Most SUSY-inspired NP signatures also include substantial missing transverse energy (E_T^{miss}), corresponding to the presence of the undetected lightest SUSY particles (LSP), as well as hadronic activity in the form of jets, which arise from the decays of squarks or gluinos. As a measure of hadronic activity, we define $H_T = \sum_j p_T^j$, where the sum is over all jets with $p_T > 30$ GeV.

This analysis divides the plane of E_T^{miss} *vs.* H_T into several search regions rather than limiting the searches to very high E_T^{miss} and H_T values. The binned approach provides good sensitivity to signal events in the high E_T^{miss} and high H_T regions, which are nearly free of background and probe models with large mass splittings, while retaining sensitivity to models with smaller mass splittings that populate lower E_T^{miss} and H_T regions.

Trilepton searches with b-tagged jets, H_T, and E_T^{miss} have already been studied in more general CMS analyses which focus on all possible trilepton signatures [10, 11]. To date, these searches have not reported any excesses above the SM expectation, and thus have been used to place constraints on the SUSY particle masses. To improve the sensitivity of this analysis to new physics processes, we study the trilepton event sample as a function of the number of jets and the number of b-tagged jets.

A similar search has been performed by ATLAS collaboration using a dataset corresponding to an integrated luminosity of 13.0 fb^{-1} [12]. It reports results consistent with the SM, and probes gluino masses of up to 860 GeV and bottom squark masses up to 430 GeV.

2 Reconstruction of Leptons, Missing Energy, and Jets

Events are selected with at least three charged lepton (electron or muon) candidates that satisfy $|\eta| < 2.4$ and $p_T > 10$ GeV. Muons are reconstructed from a seed track in the muon detector combined with silicon strip and pixel information using a global fit [19]. Muon candidates from decays in flight of hadrons and punch-through particles are largely rejected by a set of track quality requirements.

Electron candidates are reconstructed [20] starting from a cluster of energy deposits in the ECAL; the cluster is then matched to hits in the silicon tracker. A selection using electron identification variables based on shower shape and track-cluster matching is applied to the reconstructed candidates; the criteria are designed to have maximum rejection of electron candidates from QCD multijet production while maintaining approximately 90% efficiency for electrons from the decay of W/Z bosons. Electron candidates satisfying $\Delta R \equiv \sqrt{\Delta\phi^2 + \Delta\eta^2} < 0.1$ with any of the selected muons are rejected to suppress background from muon bremsstrahlung and final-state radiation. Electron candidates originating from photon conversions are suppressed by looking for a partner track and requiring no missing hits for the track fit in the inner layers of the tracking detectors.

Charged leptons (ℓ) produced in the decays of heavy particles, including W and Z bosons as well as SUSY particles, are typically spatially isolated from the hadronic activity in the event. In contrast, leptons produced in the decays of hadrons, as well as hadrons misidentified as leptons, are typically embedded in jets. To distinguish between the leptons from signal and background processes, we therefore define an isolation quantity, I_{rel}, as the ratio of the scalar sum of transverse momenta of the charged and neutral hadrons and photons within a cone of $\Delta R < 0.3$ around the lepton candidate direction at the origin, to the transverse momentum of the candidate. The contribution from the candidate itself is excluded. Electrons and muons with $I_{rel} < 0.15$ are considered isolated.

In order to further suppress the background from leptons produced in the decays of heavy-flavor hadrons, we reject leptons with large transverse impact parameter with respect to the reconstructed vertex of the pp collision and require all leptons to be consistent with originating from a common interaction vertex.

Jets and E_T^{miss} are reconstructed using the particle-flow technique [21, 22]. For jet clustering, we use the anti-k_T algorithm with the distance parameter 0.5 [23]. Jets are required to pass standard quality requirements [24] to remove those consistent with calorimeter noise. After the expected contribution from extra pp collisions in the same beam crossing is subtracted, jet energies are corrected for residual non-uniformity and nonlinearity of the detector response using corrections found with collision data [25]. We require jets to have $p_T > 30$ GeV and $|\eta| < 2.4$

to be considered for analysis. Furthermore, we use standard b-jet identification criteria that provide around 70% efficiency with less than 1% mis-tag rate [26]. Jets that are within a cone of $\Delta R < 0.4$ around lepton candidates that pass all the criteria above are removed, except in the case that the jet is b-tagged; in this case the lepton is not considered to be isolated and is included as part of the b-tagged jet. This requirement acts as an additional isolation requirement on the leptons and reduces the dominant background, $\mathrm{t\bar{t}}$ production, by 25-40% depending on the search region compared to the case where such an object is reconstructed as a lepton rather than a b-tagged jet. The decrease of the prompt lepton efficiency due to this requirement is found, using Drell-Yan (DY) events in both data and simulation, to be well below 1%.

The missing transverse energy is computed as the negative vector sum of the transverse momenta of the Particle Flow objects in the event.

3 Event Selection, Search Regions and Event Simulation

The online event selection is performed using triggers that require the presence of two high p_{T} leptons (with $p_{\mathrm{T}} > 8$ GeV and $p_{\mathrm{T}} > 17$ GeV); for electron candidates the trigger also applies isolation requirements. Events with trileptons selected by the analysis pass this online selection with close to 100% efficiency. The offline selection begins with a requirement that three leptons are reconstructed and pass the full selection requirements, including isolation. We require that the three leptons each have $p_{\mathrm{T}} > 10$ GeV, including at least one with $p_{\mathrm{T}} > 20$ GeV, where the trigger is fully efficient.

Since the signal models of interest have multiple jets and multiple b-jets, events are required to have at least two jets and at least one b-tagged jet.

A sideband sample is defined in which the events satisfy all of the selection requirements, except that one of the three leptons is not isolated ($I_{\mathrm{rel}} > 0.15$). This sideband region is used to estimate the background from processes with two prompt leptons and one non-prompt or misidentified lepton (e.g. from DY+jets and $\mathrm{t\bar{t}}$).

At this stage we split the selected event sample into two categories depending on whether or not two of the leptons constitute a Z boson candidate. Events with a pair of oppositely charged leptons of the same flavor (OSSF) are classified as either On-Z, if the invariant mass of the dilepton system is in the range 75-105 GeV, or Off-Z, if the invariant mass is outside of this range. The Off-Z sample also includes events without an OSSF lepton pair. To suppress background from heavy-flavor decays and low-mass DY production, the invariant mass of each opposite-sign dilepton system is required to be greater than 12 GeV.

The requirement $E_{\mathrm{T}}^{\mathrm{miss}} > 50$ GeV is imposed to select events with significant transverse energy associated with unobserved particles. This requirement is expected to be nearly 100% efficient for any of the signal models under consideration. For example, in model A1 (Fig. 1a) with $\mathrm{m}_{\tilde{\mathrm{g}}} = 900$ GeV and $\mathrm{m}_{\tilde{\chi}_1^0} = 100$ GeV, the mean $E_{\mathrm{T}}^{\mathrm{miss}}$ is 240 GeV, and the efficiency for $E_{\mathrm{T}}^{\mathrm{miss}} > 50$ GeV is 96%.

Once this baseline selection is imposed, the yields are reduced to 73 events (On-Z) and 90 events (Off-Z). Figure 4 shows the distribution of events observed in data across the plane of $E_{\mathrm{T}}^{\mathrm{miss}}$ *vs.* H_{T} with the requirement $E_{\mathrm{T}}^{\mathrm{miss}} > 50$ GeV removed. The search regions are delineated by dashed lines. As expected, the vast majority of events occupy the low $E_{\mathrm{T}}^{\mathrm{miss}}$, low H_{T} regions, with a small number of outliers being present in the other search regions. The remaining SM processes that give significant background are top-pair production, top-pair production in association with bosons ($\mathrm{t\bar{t}V}$), and multi-boson (WZ, ZZ) production. The fundamental chal-

lenge of the analysis is to determine whether or not our understanding of the SM can account for these observed yields.

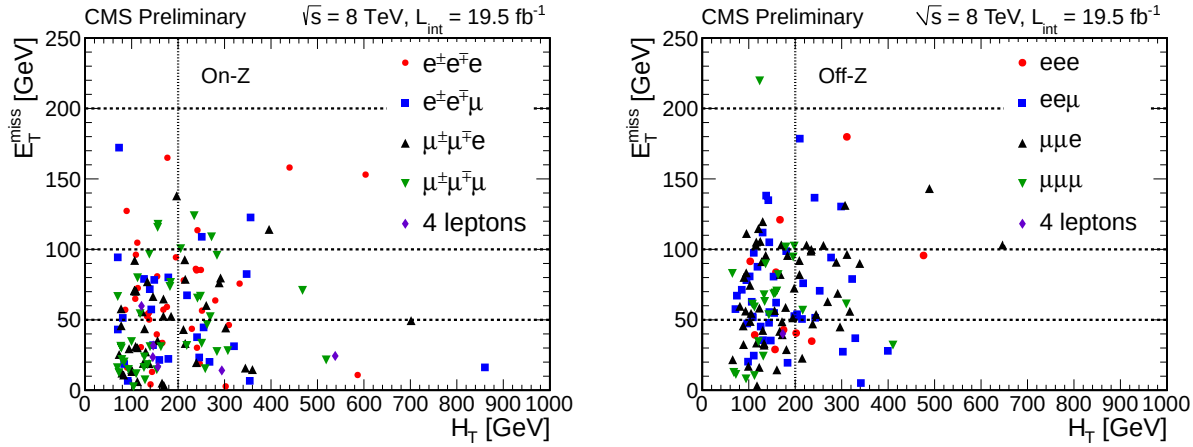

Figure 4: Distribution of events after the baseline event selection in data in the $E_{\mathrm{T}}^{\mathrm{miss}}$ *vs.* H_{T} plane for On-Z (left) and Off-Z (right) categories. The requirement $E_{\mathrm{T}}^{\mathrm{miss}} > 50$ GeV has not been applied to illustrate the background population at low $E_{\mathrm{T}}^{\mathrm{miss}}$.

To improve the sensitivity to signal events, the sample obtained with the baseline event selection is divided into multiple search regions (SR), defined using an additional set of kinematic variables: the number of jets, the number of b-quark jets, $E_{\mathrm{T}}^{\mathrm{miss}}$, and H_{T}. The set of the kinematic variables as well as the boundaries defining each search region were chosen and optimized with the simulation to have the best discovery potential. For the signal models of interest, high (b-quark) jet multiplicity and high-H_{T} and $E_{\mathrm{T}}^{\mathrm{miss}}$ regions are expected to provide the best sensitivity. Table 1 defines a set of search regions in terms of the requirements for each of these variables. There are a total of 60 search regions, 30 each for On-Z and Off-Z, specified by the different combinations of requirements listed in Table 1. For the On-Z sample with $\mathrm{N_{b\text{-}jets}}$=1, there are 12 possible regions based on the remaining kinematic variables. For $\mathrm{N_{b\text{-}jets}} \geq$3, the SM background is negligible, so the two $\mathrm{N_{jets}}$ bins are combined.

Table 1: Binning defining the baseline selection and the search regions (SR) of the analysis. All the combinations of these requirements are used to create the 60 SR. For $\mathrm{N_{b\text{-}jets}} \geq 3$ no extra jet multiplicity binning is added.

Variable	Baseline	Search Regions		
Sign/Flavor	3 e/μ	On-Z	Off-Z	
$\mathrm{N_{b\text{-}jets}}$	≥ 1	1	2	≥ 3
$\mathrm{N_{jets}}$	≥ 2	2–3	≥ 4	
H_{T} (GeV)	≥ 60	60–200	≥ 200	
$E_{\mathrm{T}}^{\mathrm{miss}}$ (GeV)	≥ 50	50–100	100–200	≥ 200

Monte Carlo (MC) simulations are used for studies of the properties of signal and SM background processes. The SM samples (i.e. WZ, $\mathrm{t\bar{t}W}$, $\mathrm{t\bar{t}Z}$, $\mathrm{t\bar{t}H}$, $\mathrm{t\bar{b}Z}$ and others) are produced at the parton level with the MADGRAPH 5 v1.1.0 [27] event generator using the CTEQ 6L1 [28] parton distribution functions. Parton showering and hadronization are carried out with the PYTHIA 6.424 [29] program. The detector response is modeled with the GEANT4 [30] program,

followed by the same event reconstruction as the one used for data. The most accurate calculations of the cross sections available are used for the SM samples normalization, mostly with the next-to-leading order (NLO) or the next-to-next-to-leading order (NNLO) precision [31–34].

Signal samples are produced for a range of gluino (sbottom) and LSP (chargino) masses with the MADGRAPH 5 v1.5.4 [27] event generator; up to two partons are present in addition to the gluino (sbottom) pair. PYTHIA 6.424 [29] is used to simulate parton showering and hadronization. The detector response and reconstruction are produced with the CMS fast simulation framework [35]. The small differences between the GEANT4 and the fast simulations are corrected for in the analysis. The gluino (sbottom) pair production cross-sections are calculated including the resummation of soft gluon emission at the next-to-leading logarithmic accuracy whenever available, otherwise they are derived with the next-to-leading order in the strong coupling constant [36–41].

4 Methods for Background Predictions

The backgrounds in this search are small in general, but come from a variety of sources. We separate these into three categories: (a) events with one or more non-prompt or misidentified leptons, (b) events with three prompt leptons from diboson (WZ and ZZ) production, and (c) events with three prompt leptons from rare SM processes such as $t\bar{t}$+V, $t\bar{t}$+H, $t\bar{b}$+Z, VVV, where V denotes either the W or Z boson.

Non-prompt or misidentified leptons come mainly from top quark production as well as from Z+jets and WW+jets events. As a consequence of the b-jet requirement, top pair production is the main source of background in many of the search regions. A data-driven technique is used to predict this background. First, the probability for a lepton from a b-tagged jet to satisfy the isolation criteria is measured in a QCD control sample in data. This sample is defined by requiring a high p_{T} b-jet ($p_{\mathrm{T}} > 40$ GeV) and a lepton opposite to it ($\Delta\phi_{\ell,\text{b-jet}} > 2$). The lepton is required to satisfy all selection criteria except for the isolation requirement. Using this sample, we measure the probability for non-prompt leptons to pass the isolation requirement. This probability is parametrized as a function of lepton transverse momentum. We then use this probability to extrapolate from the sideband region to our signal region. Values for this probability are close to 5% for muons and to 10% for electrons. This method is a variation on similar methods that have been used in CMS to predict the rates of non-prompt or misidentified leptons from backgrounds dominated by heavy flavor decays [9]. Based on performance studies of the technique in simulation, which include the level of agreement between the observed and the expected numbers of events in all search regions, we estimate a systematic uncertainty of 30% for this background determination. This incorporates the uncertainty arising from the fact that this probability is measured in a QCD-dominated control sample but applied to a different environment where the spectrum of the b-jets is harder.

The requirements of at least one identified b-jet and minimum $E_{\mathrm{T}}^{\mathrm{miss}}$ significantly reduce the backgrounds arising from diboson production. This background is estimated using simulation. The overall performance of this prediction method is checked using control samples in data where the b-jet requirement is inverted. To define a control sample sensitive to the WZ background, events are selected with three high-p_{T} leptons, where the invariant mass of an OSSF dilepton system is consistent with the Z boson mass. In addition, the events in the control sample are required to have significant missing energy (50 GeV$< E_{\mathrm{T}}^{\mathrm{miss}} <$100 GeV), and the transverse mass of the system comprising the third lepton (the one not used in the Z) and the missing transverse energy is required to satisfy 50 GeV$<M_T<$120 GeV. For the control sample of the ZZ background, four isolated and identified leptons, of which two form a Z candidate,

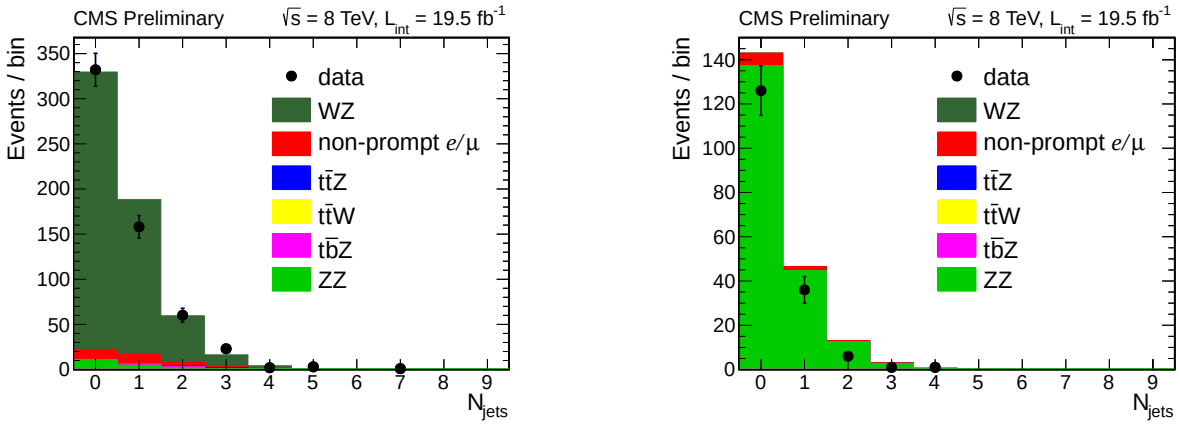

Figure 5: Jet multiplicity distributions for diboson events in WZ (left) and ZZ (right) control regions in data and simulated event samples.

are selected. In addition, the events are required to have $E_{\mathrm{T}}^{\mathrm{miss}} < 50$ GeV. The jet multiplicity distributions in both control regions are displayed in Fig. 5. Reasonable agreement between the shapes and the normalizations of the distributions in simulation and observed data is obtained. A scale factor of 0.89 is derived for ZZ yield based on the observed and predicted yields in the control region. Given that the estimation of these processes from simulation relies on the modeled distribution of additional partons needed to yield a b-jet, we assign a 50% uncertainty on the diboson background to account for inability to verify the simulation performance at this level.

In many of the search regions, certain rare, but irreducible Standard Model processes play a significant role. For example the production of top quarks in association with vector bosons (e.g., $\mathrm{t\bar{t}Z}$) is an important source of background. Because of its small cross section, this process only recently became accessible to measurement at hadron colliders and therefore has not been studied in detail. The On-Z region with at least 1 b-tagged jet and high jet multiplicity can be used for cross-checking these processes, since it contains mainly $\mathrm{t\bar{t}Z}$ events. Other rare processes, such as triboson production, are strongly suppressed because of the requirement of having at least 1 b-tagged jet. For all these backgrounds, the simulation is used to predict the shape and yields. A 50% systematic uncertainty is assigned to account for the limited experimental cross-checks possible for these processes.

5 Results

Figures 6a and 6b show the missing transverse energy spectrum and the jet and b-jet multiplicity distributions for the Off-Z and On-Z regions, respectively. The contribution from non-prompt and misidentified leptons (mainly from $\mathrm{t\bar{t}}$ events) is the dominant background and is estimated from control samples in the data, while the other backgrounds are predicted using simulation as described in Section 4.

The $E_{\mathrm{T}}^{\mathrm{miss}}$ spectrum in bins of jet and b-jet multiplicity can be seen in Fig. 7 for the three-lepton results without a Z candidate, and in Fig. 8 for those with a Z candidate. The search regions with higher jet and b-jet multiplicity have less SM background, but the signal efficiency diminishes as well. In order to maximize the sensitivity to a variety of models, we perform a simultaneous multi-bin fit to obtain the final upper limits on the cross-section times branching fraction ($\sigma \times BF$) of the models described in the introduction and shown Figures 1, 2, and 3.

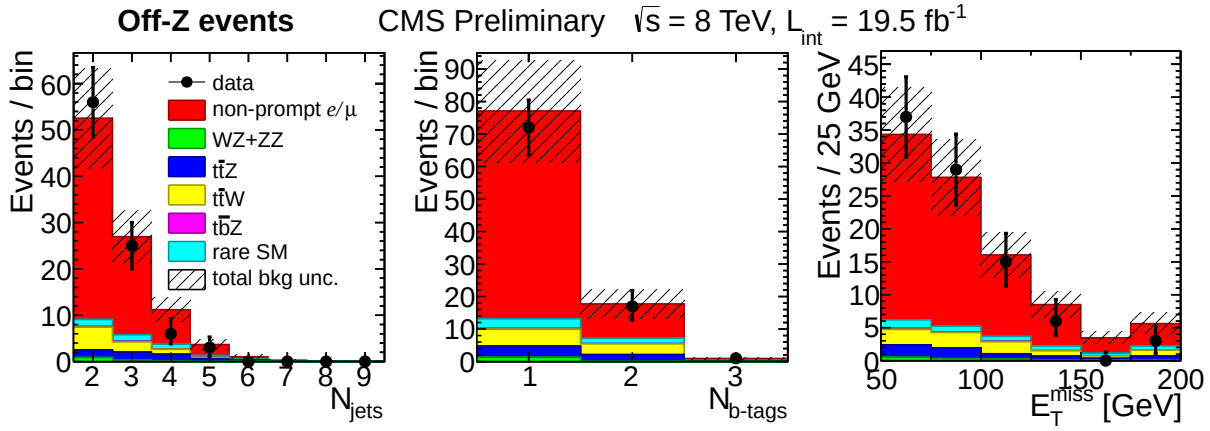

(a) Off-Z

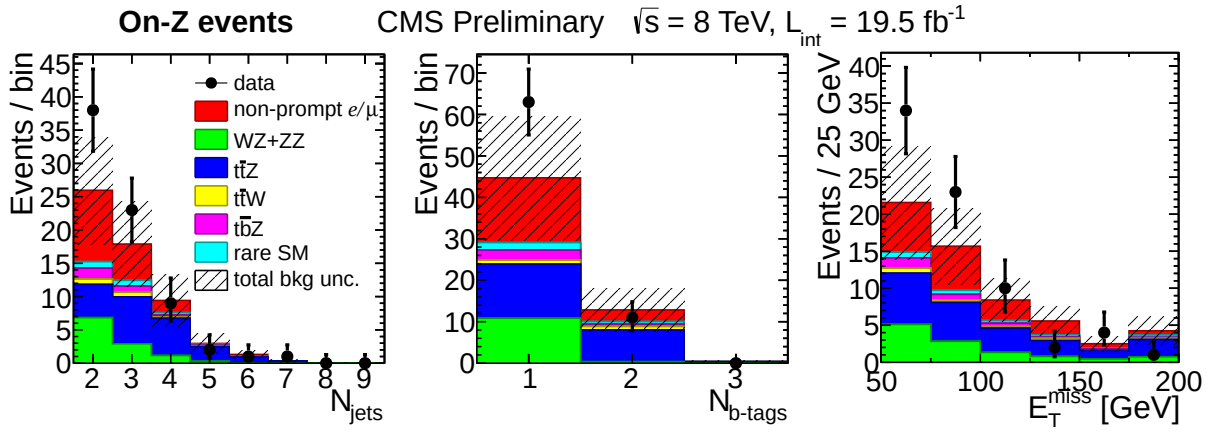

(b) On-Z

Figure 6: Observed data events and predicted SM background as a function of number of jets, $E_{\mathrm{T}}^{\mathrm{miss}}$, H_{T}, and number of b-jets are shown for events that (a) do not contain or (b) contain an opposite-sign-same-flavor pair that is a Z boson candidate. The last bin in the histograms includes overflow events. The shaded bands correspond to the estimated uncertainties on the background which are calculated on the per bin basis.

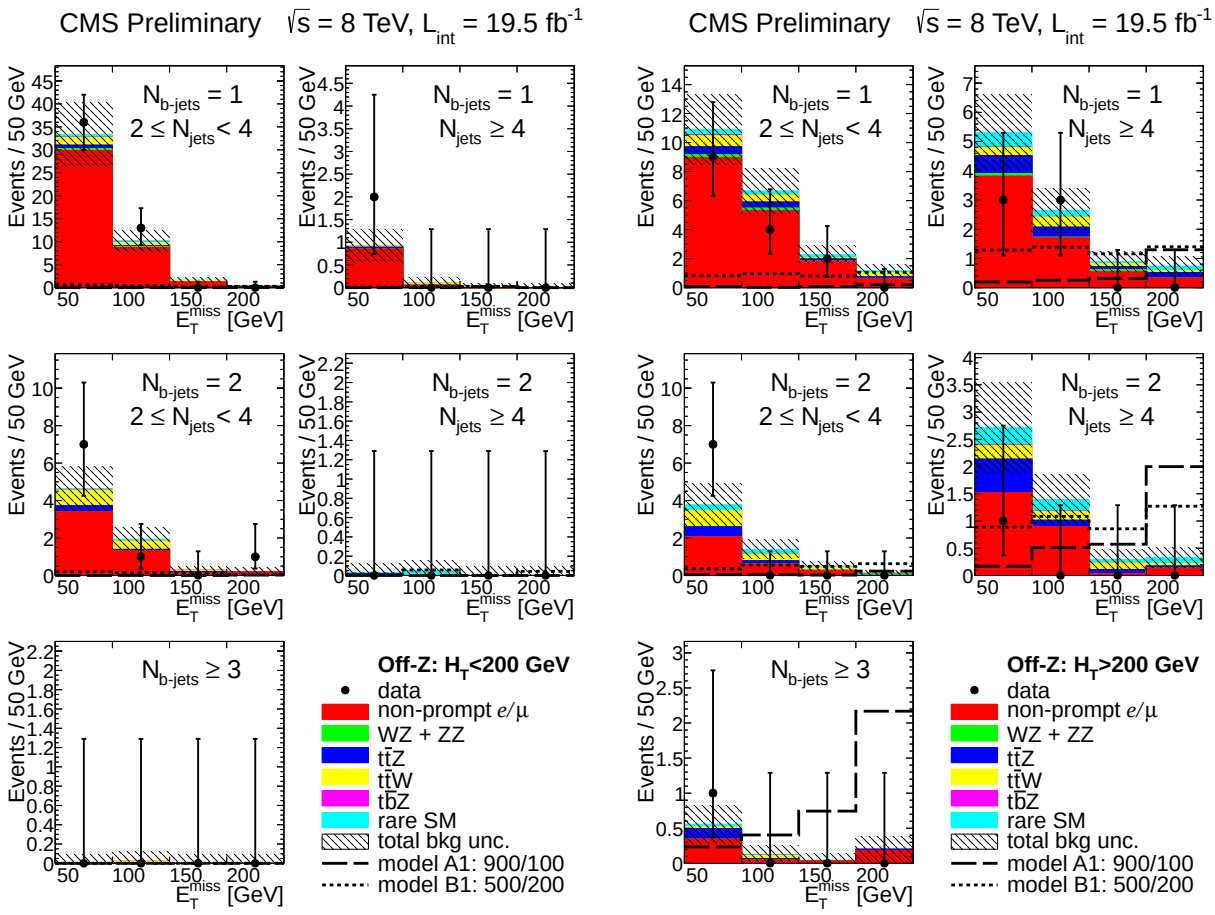

(a) Low H_T (b) High H_T

Figure 7: Predicted total background and observed data yields as a function of E_T^{miss} for events that do not contain an opposite-sign-same-flavor pair that is a Z boson candidate (Off-Z): (a) $H_T < 200$ GeV and (b) $H_T > 200$ GeV. The shaded bands correspond to the estimated uncertainties on the background. The dashed histograms show an expected yield for the A1 model with particle masses $m_{\tilde{g}} = 900$ GeV and $m_{\tilde{\chi}_1^0} = 100$ GeV. The dotted histograms show an expected yield for the B1 model with particle masses $m_{\tilde{b}} = 500$ GeV and $m_{\tilde{\chi}^\pm} = 200$ GeV.

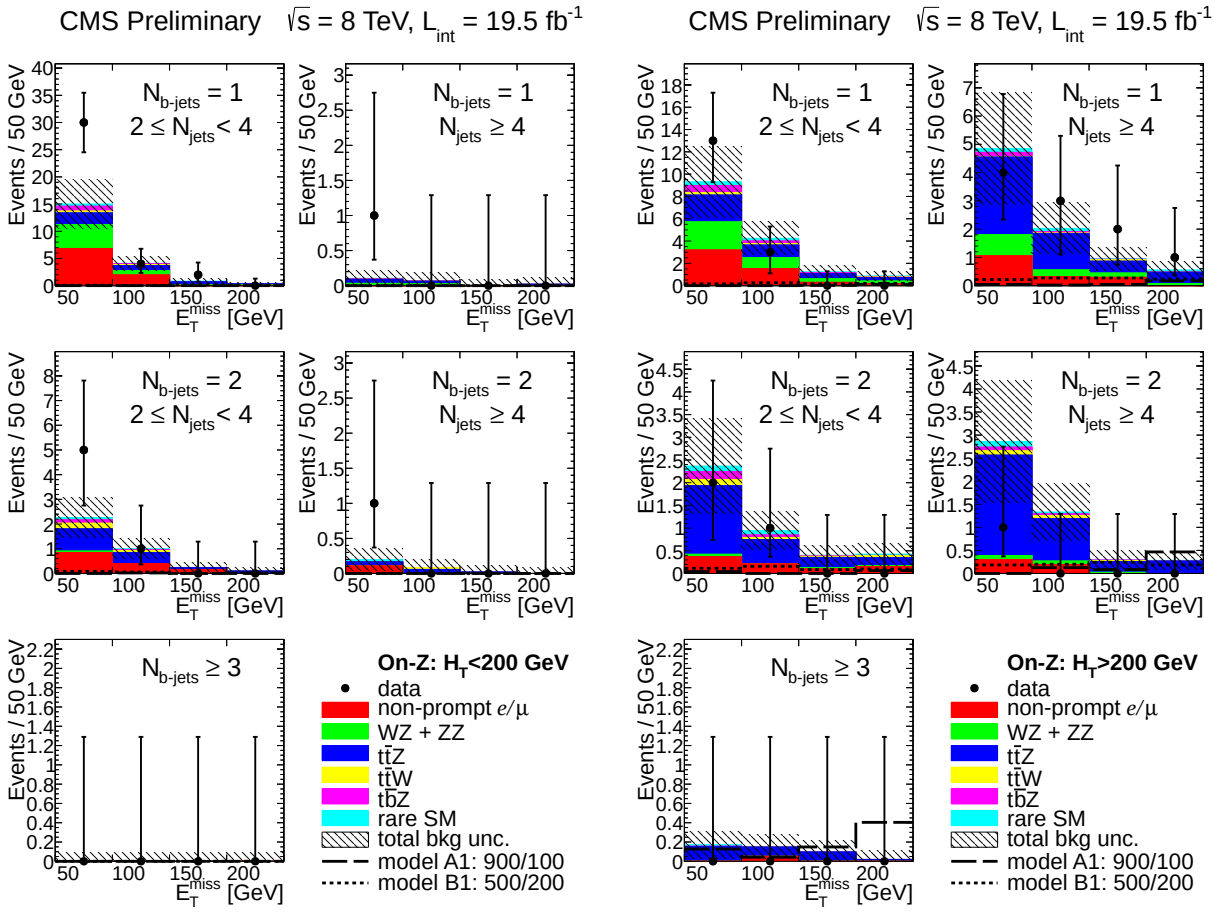

(a) Low H_T (b) High H_T

Figure 8: Predicted total background and observed data yields as a function of E_T^{miss} for events that contain an opposite-sign-same-flavor pair that is a Z boson candidate (On-Z): (a) $H_T < 200$ GeV and (b) $H_T > 200$ GeV. The shaded bands correspond to the estimated uncertainties on the background. The dashed histograms show an expected yield for the A1 model with particle masses $m_{\tilde{g}} = 900$ GeV and $m_{\tilde{\chi}_1^0} = 100$ GeV. The dotted histograms show an expected yield for the B1 model with particle masses $m_{\tilde{b}} = 500$ GeV and $m_{\tilde{\chi}^\pm} = 200$ GeV.

Table 2: Predicted total background and observed data yields as a function of E_T^{miss} for events with no Z candidate present (Off-Z). Upper limits (68% CL) are quoted when there is not enough events in data and simulation to derive an expected number of background events.

$N_{b\text{-tags}}$	N_{jets}	E_T^{miss} (GeV)	$H_T < 200$ GeV		$H_T > 200$ GeV	
			Expected	Observed	Expected	Observed
1	2–3	50–100	33.3 ± 7.0	36	10.9 ± 2.4	9
		100–200	11.8 ± 2.6	13	9.0 ± 2.0	6
		$\geq$200	0.33 ± 0.21	0	1.2 ± 0.4	0
	$\geq$4	50–100	0.92 ± 0.36	2	5.3 ± 1.3	3
		100–200	0.10 ± 0.12	0	3.5 ± 1.0	3
		$\geq$200	< 0.09	0	0.74 ± 0.31	0
2	2–3	50–100	4.7 ± 1.9	7	3.8 ± 1.1	7
		100–200	2.2 ± 0.7	1	1.9 ± 0.7	0
		$\geq$200	0.22 ± 0.19	1	0.14 ± 0.13	0
	$\geq$4	50–100	< 0.13	0	2.7 ± 0.8	1
		100–200	< 0.16	0	1.7 ± 0.6	0
		$\geq$200	< 0.09	0	0.33 ± 0.18	0
$\geq$3		50–100	< 0.09	0	0.56 ± 0.27	1
		100–200	< 0.12	0	0.17 ± 0.13	0
		$\geq$200	< 0.09	0	0.20 ± 0.19	0

Table 3: Predicted total background and observed data yields as a function of E_T^{miss} for events with a Z candidate present (On-Z). Upper limits (68% CL) are quoted when there is not enough events in data and simulation to derive an expected number of background events.

$N_{b\text{-tags}}$	N_{jets}	E_T^{miss} (GeV)	$H_T < 200$ GeV		$H_T > 200$ GeV	
			Expected	Observed	Expected	Observed
1	2–3	50–100	15.0 ± 4.5	30	9.3 ± 3.2	13
		100–200	5.0 ± 1.7	6	5.5 ± 2.0	3
		$\geq$200	0.36 ± 0.22	0	0.9 ± 0.4	0
	$\geq$4	50–100	0.11 ± 0.12	1	4.9 ± 2.0	4
		100–200	< 0.19	0	3.0 ± 1.3	5
		$\geq$200	< 0.11	0	0.56 ± 0.31	1
2	2–3	50–100	2.3 ± 0.8	5	2.6 ± 1.0	2
		100–200	1.3 ± 0.5	1	1.3 ± 0.6	1
		$\geq$200	0.12 ± 0.12	0	0.46 ± 0.24	0
	$\geq$4	50–100	0.20 ± 0.16	1	2.9 ± 1.3	1
		100–200	< 0.22	0	1.6 ± 0.8	0
		$\geq$200	< 0.09	0	0.29 ± 0.19	0
$\geq$3		50–100	< 0.09	0	0.17 ± 0.14	0
		100–200	< 0.09	0	0.25 ± 0.16	0
		$\geq$200	< 0.09	0	0.02 ± 0.09	0

Table 4: Systematic uncertainties on the signal acceptance.

Source	Uncertainty, %
Luminosity	4.4
Modeling of lepton reconstruction, ID, I_{rel} based on Z-events	12
Jet energy scale	5–15
Unclustered energy and lepton effects on $E_{\text{T}}^{\text{miss}}$	5
Modeling of b-jet multiplicity	5–20
Trigger	5
Total systematic uncertainty	15–30

Tables 2 and 3 summarize the expected backgrounds and observed yields in data. The uncertainties quoted in the tables represent the total uncertainty, which is dominated by its statistical component in most signal regions. Within the uncertainties, agreement is observed between the data and the predicted backgrounds in most of the search regions.

One of the search regions in the On-Z samples has a 1.9 σ excess (30 observed *vs.* 15.0$\pm$4.5 expected). Cross-checks performed on this region indicate that a statistical fluctuation of the background is the most plausible explanation.

6 Interpretation

The results are interpreted in several simplified models [42–46]:

- gluino-pair production with gluinos decaying through a top squark, $\text{pp} \to \tilde{\text{g}}\tilde{\text{g}} \to \text{t}\bar{\text{t}}\text{t}\bar{\text{t}}\tilde{\chi}_1^0\tilde{\chi}_1^0$. The top squark can be either off-shell (model A1) or on-shell (model A2).
- direct sbottom-pair production (model B1) or gluino-pair production with $\tilde{\text{g}} \to \tilde{\text{b}}_1\bar{\text{b}}$ (model B2) followed by sbottom decay to a chargino and a top quark, where the chargino undergoes the decay to the W boson and the lightest neutralino: $\text{pp} \to \tilde{\text{b}}_1\tilde{\text{b}}_1^* \to \text{t}\bar{\text{t}}\text{WW}\tilde{\chi}_1^0\tilde{\chi}_1^0$ for the model B1 and $\text{pp} \to \tilde{\text{g}}\tilde{\text{g}} \to \text{b}\bar{\text{b}}\text{t}\bar{\text{t}}\text{WW}\tilde{\chi}_1^0\tilde{\chi}_1^0$ for the model B2.
- direct $\tilde{\text{b}}_1$-pair production, where $\tilde{\text{b}}_1$ decays to a b-quark and a $\tilde{\chi}_2^0$, followed by its decay to a Z and a $\tilde{\chi}_1^0$: $\text{pp} \to \tilde{\text{b}}_1\tilde{\text{b}}_1^* \to \text{b}\bar{\text{b}}\text{ZZ}\tilde{\chi}_1^0\tilde{\chi}_1^0$ (model C1).

6.1 Signal Acceptance Uncertainties

Table 4 summarizes the systematic uncertainties on the signal acceptance. The recorded luminosity of the CMS experiment is known to 4.4% precision [47]. The lepton selection efficiency is studied using a standard tag-and-probe technique in data and simulation using Z events. The uncertainty on the lepton reconstruction efficiency is 3% and is obtained from studies of leptonic Z-boson decays. Extra studies were done to quantify the influence of the large hadronic activity on the lepton isolation. Combining the two sources leads to around 12% uncertainty on the three-lepton selection. The systematic uncertainty on the trigger efficiency is very small, because dilepton triggers are used for a trilepton signature and thus the trigger efficiency is always very close to 100%. Other sources of systematic uncertainty are the jet energy scale, the modeling of the underlying event, and the b-tagging efficiency. Some uncertainties can only be quantified when a signal model of interest is specified and the final state topologies and kinematics are studied, therefore a lower bound on the signal acceptance uncertainty of 15-30% is given.

6.2 Limit Setting Procedure

The upper limits (95% CL) on the signal rate are calculated using the modified frequentist CL_s method [48–50]. The results of all search regions are taken into account in order to maximize sensitivity. Formally, we construct a likelihood function,

$$\mathcal{L}(\text{data}|\mu,\theta) = \text{Poisson}\left(\text{data}|\mu\cdot s(\theta)+b(\theta)\right)\cdot p\left(\hat{\theta}|\theta\right), \quad (1)$$

where "data" represents our observed yields, and Poisson(data| μ,θ) represents the product of probabilities to observe n_i events in the ith search region (SR), i.e.,

$$\text{Poisson}(\text{data}|\mu,\theta) = \prod_i \frac{(\mu s_i + b_i)^{n_i}}{n_i!} e^{-(\mu s_i + b_i)}. \quad (2)$$

Here, the parameter μ represents our signal strength modifier and determines the quantity $\sigma \times BF$ in the context of the CMS Simplified Model interpretations. The parameter θ denotes the collection of nuisance parameters that can influence the values of b and s. Log-normal probability density functions ($p\left(\hat{\theta}|\theta\right)$) are assumed for both the signal and background nuisance parameters. These are taken to be either 0% or 100% correlated as appropriate. The profile likelihood ratio is used to test the compatibility of the observed data with the background-only and signal+background hypotheses. The full prescription can be found elsewhere [50].

6.3 Limits

The results from the off-Z search regions are used to set constraints on the models A1 – B2, and from the on-Z search regions for the model C1.

The expected (red dashed) and observed upper limits (black solid) on gluino and LSP (or top squark) masses for gluino-pair production, pp $\to \widetilde{g}\widetilde{g} \to t\bar{t}t\bar{t}\widetilde{\chi}_1^0\widetilde{\chi}_1^0$, are shown in Fig. 9. Figure 9a corresponds to the model A1, and Fig. 9b to the model A2. Gluino masses up to 975 (900) GeV are excluded across the range of LSP masses down to $\Delta M_{\widetilde{g},\widetilde{\chi}_1^0} = 425(350)$ GeV in case of very heavy top squarks; and up to 1000 GeV across the range of top squark masses from 250 to 800 GeV in case of LSP mass equal to 50 GeV. The search regions which have the most sensitivity are these with high b-jet multiplicity ($N_{\text{b-jets}} = 2$ and $N_{\text{b-jets}} \geq 3$), high jet multiplicity ($N_{\text{jets}} \geq 4$), high hadronic activity ($H_T > 200$ GeV) and medium (100–200 GeV) or high (> 200 GeV) missing transverse energy.

Figure 10 shows the expected (red dashed) and observed upper limits (black solid) on gluino and bottom squark masses for the gluino-mediated sbottom production accompanied by a b-quark emission and followed by subsequent decays to chargino and top-quark (model B2). Gluino masses up to 1000 GeV are excluded for sbottom masses from 400 to 950 GeV, chargino mass 150 GeV and LSP mass 50 GeV (Fig. 10a); and up to the same value for the case when chargino mass is fixed to 300 GeV (Fig. 10b). The most sensitive search regions are the same as for the models A1 and A2.

Figure 11 shows the expected (red dashed) and observed upper limits (black solid) on bottom squark mass for direct sbottom production followed by subsequent decays to chargino and top-quark, pp $\to \widetilde{b}_1\widetilde{b}_1^* \to t\bar{t}WW\widetilde{\chi}_1^0\widetilde{\chi}_1^0$ (model B1). Three parameterizations for this model are considered.

- Mass of the LSP is fixed to 50 GeV: sbottom masses up to 575 GeV are excluded for the range of chargino masses from 150 to 375 GeV (Fig. 11a).
- The ratio $m_{\widetilde{\chi}_1^0}/m_{\widetilde{\chi}^\pm}$ is fixed to 0.5: sbottom masses up to 575 GeV are excluded for LSP mass between 25 and 150 GeV (Fig. 11b).

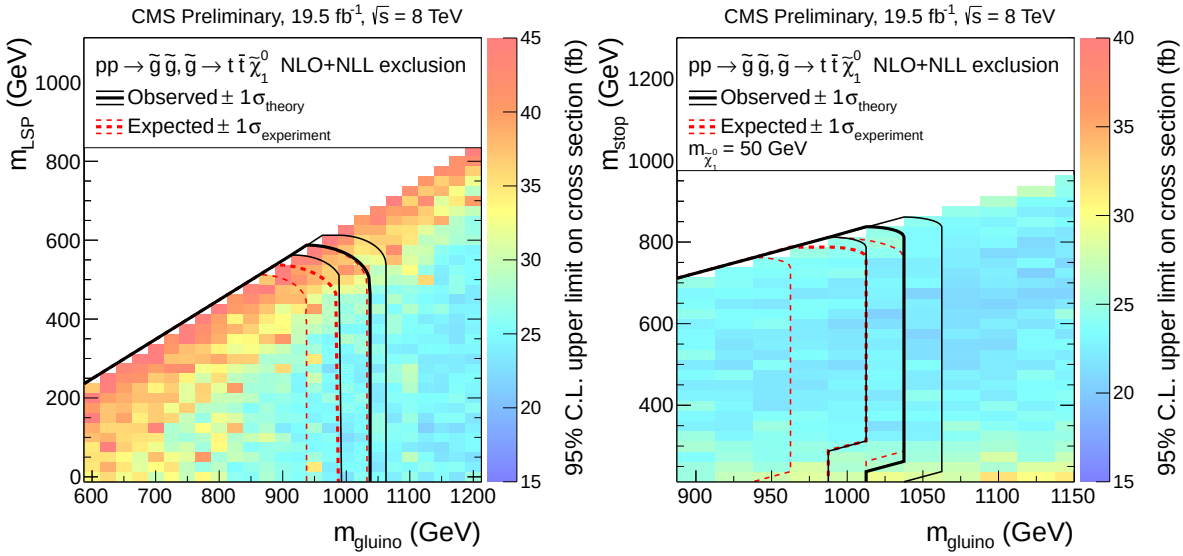

(a) Model A1 (b) Model A2

Figure 9: The 95% CL upper limits on the (a) model A1 and (b) model A2 scenario cross sections (fb) derived using the CL_s method. The solid (black) contours show the observed exclusions assuming the NLO+NLL cross sections, along with the ± 1 standard deviation theory uncertainties. The dashed (red) contours present the corresponding expected results, along with the ± 1 standard deviation experimental uncertainties.

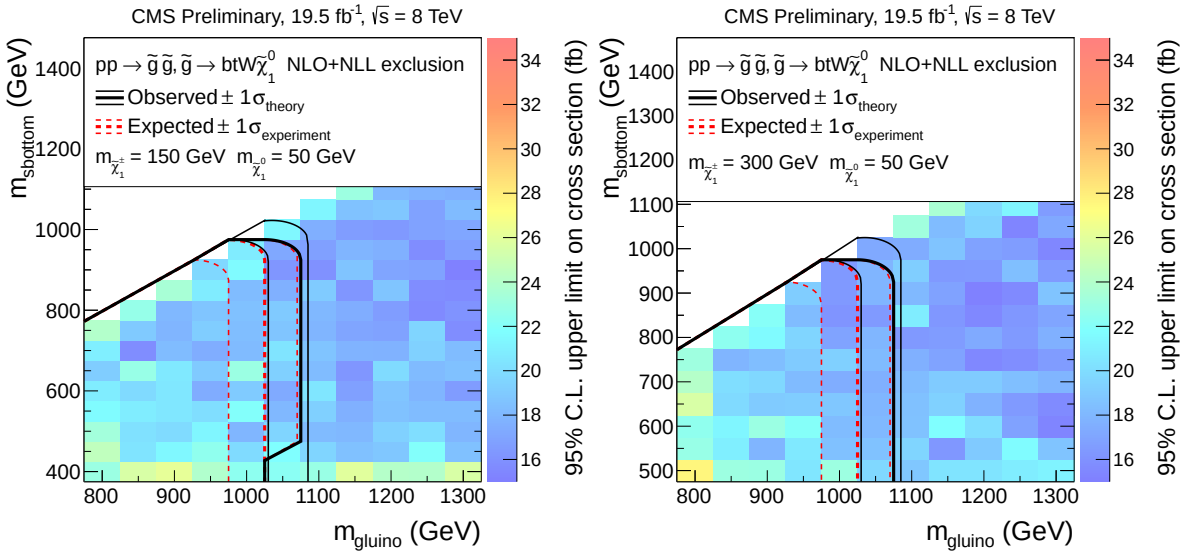

(a) Model B2: $m_{\tilde{\chi}^{\pm}} = 150$ GeV (b) Model B2: $m_{\tilde{\chi}^{\pm}} = 300$ GeV

Figure 10: The 95% CL upper limits on the model B2 scenario cross sections (fb) derived using the CL_s method. In the model B2, it is assumed that $m_{\tilde{\chi}^0_1} = 50$ GeV with (a) $m_{\tilde{\chi}^{\pm}} = 150$ GeV or (b) $m_{\tilde{\chi}^{\pm}} = 300$ GeV. The solid (black) contours show the observed exclusions assuming the NLO+NLL cross sections, along with the ± 1 standard deviation theory uncertainties. The dashed (red) contours present the corresponding expected results, along with the ± 1 standard deviation experimental uncertainties.

- The ratio $m_{\widetilde{\chi}_1^0}/m_{\widetilde{\chi}^\pm}$ is fixed to 0.8: sbottom masses up to 525 GeV are excluded for LSP mass between 25 and 200 GeV (Fig. 11c). For higher LSP masses the exclusion is less stringent.

The search regions which contribute the most to the sensitivity are the ones with $N_{\text{b-jets}} = 1$, $2 \leq N_{\text{jets}} < 4$ or $N_{\text{jets}} \geq 4$, high H_T and medium or high missing transverse energy.

The expected (red dashed) and observed upper limits (black solid) on bottom squark and LSP masses for $\widetilde{b}_1$-pair production, $pp \to \widetilde{b}_1\widetilde{b}_1^* \to b\bar{b}ZZ\widetilde{\chi}_1^0\widetilde{\chi}_1^0$, are shown in Fig. 12. In this model the mass difference between the LSP and neutralino ($m_{\widetilde{\chi}_2^0} - m_{\widetilde{\chi}_1^0}$) is set to 110 GeV, thus only the decay $\widetilde{\chi}_2^0 \to Z\widetilde{\chi}_1^0$ is kinematically allowed, while the competing decay $\widetilde{\chi}_2^0 \to h\widetilde{\chi}_1^0$ is closed. The $\widetilde{b}_1$ mass up to 450 GeV is excluded for LSP masses 100–125 GeV.

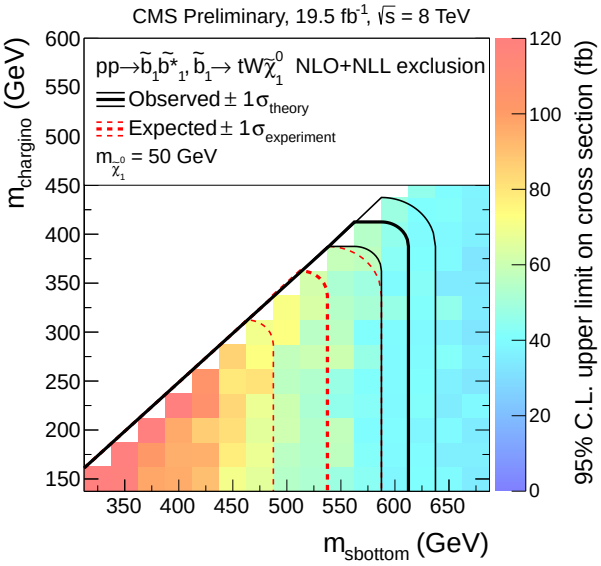

(a)

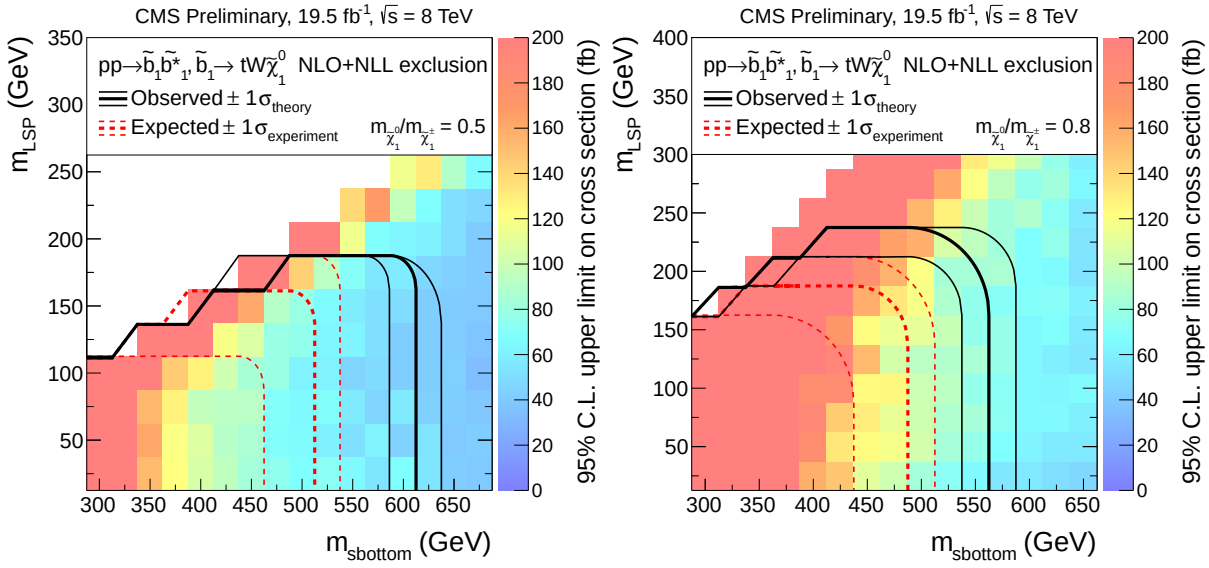

(b) (c)

Figure 11: The 95% CL upper limits on the model B1 scenario cross sections (fb) derived using the CL_s method. The limits are computed for the following scenarios within the model B1: (a) $m_{\tilde{\chi}_1^0} = 50$ GeV, (b) $m_{\tilde{\chi}_1^0}/m_{\tilde{\chi}^\pm} = 0.5$ or (c) $m_{\tilde{\chi}_1^0}/m_{\tilde{\chi}^\pm} = 0.8$. The solid (black) contours show the observed exclusions assuming the NLO+NLL cross sections, along with the ± 1 standard deviation theory uncertainties. The dashed (red) contours present the corresponding expected results, along with the ± 1 standard deviation experimental uncertainties. For the scenario (b) the deviation of the observed exclusion from the expected one is evaluated to be at the level of two standard deviations experimental uncertainties.

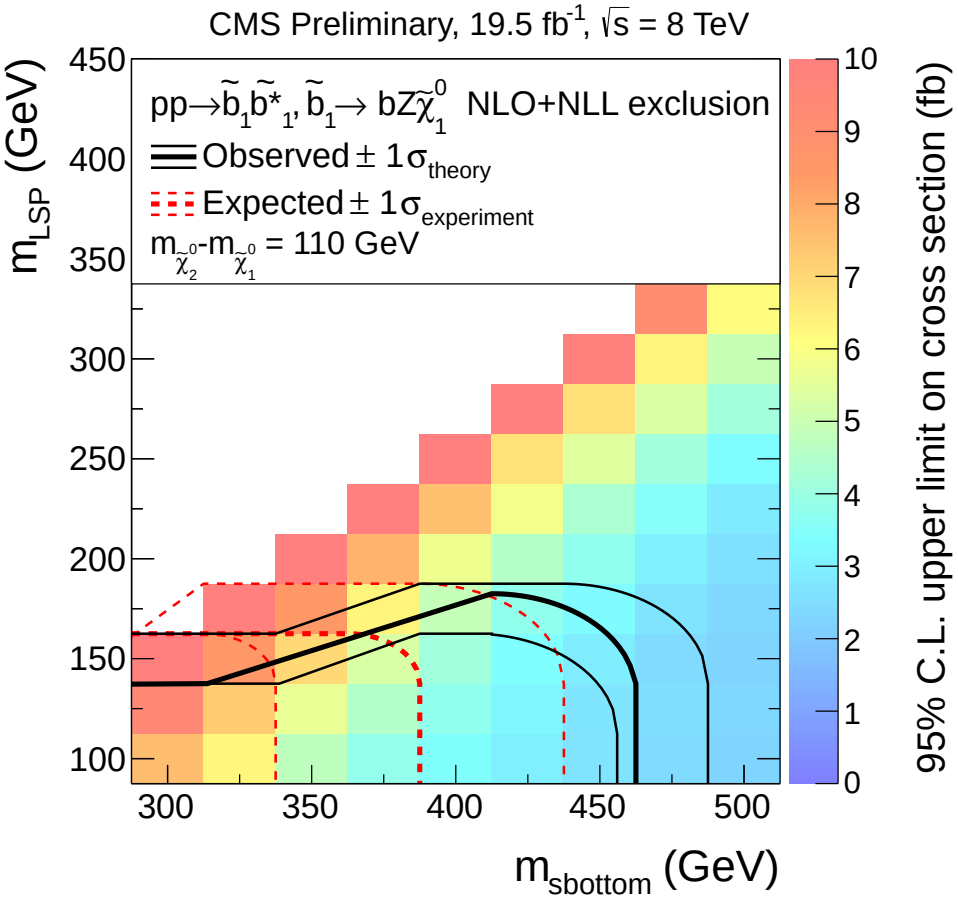

Figure 12: The 95% CL upper limits on the model C1 scenario cross sections (fb) derived using the CL_s method. The solid (black) contours show the observed exclusions assuming the NLO+NLL cross sections, along with the ± 1 standard deviation theory uncertainties. The dashed (red) contours present the corresponding expected results, along with the ± 1 standard deviation experimental uncertainties.

7 Conclusions

We present the results of a search for new physics with the signature of three leptons plus b-quarks and missing transverse energy using a dataset with an integrated luminosity of 19.5 fb^{-1} produced by the LHC with pp collisions at $\sqrt{s} = 8$ TeV.

The analysis is designed to increase sensitivity to SUSY models where multi-W or multi-Z bosons are produced in association with multi-b-quarks jets and the lightest supersymmetric particle. We predict the dominant SM background using well established data-driven techniques. To reflect several kinematic regions which could be sensitive to a range of new physics models, the various search regions are constructed. These include the search regions with or without a Z candidate present, medium or high missing transverse energy, low or high hadronic activity and (b-)jet multiplicity. We observe no statistically significant excesses of events in the signal regions in data above the SM expectations.

The results are used to place 95% CL upper limits on the cross-section times branching fraction for various simplified SUSY models. These upper limits translate into lower limits on the gluino and the sbottom mass. Gluinos decaying to top pairs and neutralinos through virtual stops are excluded for masses up to 975 (900) GeV for a range of neutralino masses from 0 to 500 (550) GeV. In case gluinos are decaying to stops with masses from 250 to 800 GeV and neutralino mass is 50 GeV, the lower limit on gluino mass reaches 1000 GeV. The same is the lower limit for gluinos which decay to sbottoms with masses from 500 to 950 GeV. The lower limit on the sbottom mass extends from 450 to 575 GeV in the considered SMS models, and it depends on the decay chains in the SMS models and on other sparticles ($\widetilde{\chi}^{\pm}$, $\widetilde{\chi}^{0}_{2}$, $\widetilde{\chi}^{0}_{1}$) masses. The limit is stronger when a sbottom undergoes a decay $\widetilde{b}_1 \to t\widetilde{\chi}^{-}$, and weaker in case of $\widetilde{b}_1 \to b\widetilde{\chi}^{0}_{2}$.

References

[1] Y. A. Golfand and E. P. Likhtman, "Extension of the algebra of Poincare group generators and violation of P invariance", *JETP Lett.* **13** (1971) 323.

[2] P. Ramond, "Dual theory for free fermions", *Phys. Rev. D* **3** (1971) 2415, doi:10.1103/PhysRevD.3.2415.

[3] A. Neveu and J. H. Schwarz, "Factorizable dual model of pions", *Nucl. Phys. B* **31** (1971) 86, doi:10.1016/0550-3213(71)90448-2.

[4] A. Neveu and J. H. Schwarz, "Quark model of dual pions", *Phys. Rev. D* **4** (1971) 1109, doi:10.1103/PhysRevD.4.1109.

[5] D. V. Volkov and V. P. Akulov, "Is the neutrino a goldstone particle?", *Phys. Lett. B* **46** (1973) 109, doi:10.1016/0370-2693(73)90490-5.

[6] J. Wess and B. Zumino, "A lagrangian model invariant under supergauge transformations", *Phys. Lett. B* **49** (1974) 52, doi:10.1016/0370-2693(74)90578-4.

[7] J. Wess and B. Zumino, "Supergauge transformations in four-dimensions", *Nucl. Phys. B* **70** (1974) 39, doi:10.1016/0550-3213(74)90355-1.

[8] Particle Data Group Collaboration, "Review of Particle Physics (RPP)", *Phys.Rev.* **D86** (2012) 010001, doi:10.1103/PhysRevD.86.010001.

[9] CMS Collaboration, "Search for supersymmetry in events with same-sign dileptons and b-tagged jets with 8 TeV data", *CMS Physics Analysis Summary* **CMS-PAS-SUS-12-029** (2012).

[10] CMS Collaboration, "Search for RPV supersymmetry with three or more leptons and b-tags", *CMS Physics Analysis Summary* **CMS-PAS-SUS-12-027** (2012).

[11] CMS Collaboration, "Search for supersymmetry in inclusive multilepton signatures", *CMS Physics Analysis Summary* **CMS-PAS-SUS-12-026** (2012).

[12] ATLAS Collaboration, "Search for supersymmetry using events with three leptons, multiple jets, and missing transverse momentum in 13.0 fb^{-1} of pp collisions with the ATLAS detector at $\sqrt{s}$=8 TeV", *ATLAS Note* **ATLAS-CONF-2012-151** (2012).

[13] S. Dimopoulos and G. Giudice, "Naturalness constraints in supersymmetric theories with nonuniversal soft terms", *Phys. Lett. B* **357** (1995) 573–578, doi:10.1016/0370-2693(95)00961-J, arXiv:hep-ph/9507282.

[14] A. G. Cohen, D. Kaplan, and A. Nelson, "The More minimal supersymmetric standard model", *Phys. Lett. B* **388** (1996) 588–598, doi:10.1016/S0370-2693(96)01183-5, arXiv:hep-ph/9607394.

[15] J. Bagger, J. L. Feng, and N. Polonsky, "Naturally heavy scalars in supersymmetric grand unified theories", *Nucl. Phys. B* **563** (1999) 3–20, doi:10.1016/S0550-3213(99)00577-5, arXiv:hep-ph/9905292.

[16] R. Barbieri and D. Pappadopulo, "S-particles at their naturalness limits", *J. High Energy Phys.* **10** (2009) 061, doi:10.1088/1126-6708/2009/10/061.

[17] M. Papucci, J. T. Ruderman, and A. Weiler, "Natural SUSY endures", *J. High Energy Phys.* **09** (2012) 035, doi:10.1007/JHEP09(2012)035.

[18] CMS Collaboration, "The CMS experiment at the CERN LHC", *JINST* **3** (2008) S08004, doi:10.1088/1748-0221/3/08/S08004.

[19] CMS Collaboration, "Performance of CMS muon reconstruction in pp collision events at $\sqrt{s} = 7$ TeV", (2012). arXiv:1206.4071. Submitted to *JINST*.

[20] CMS Collaboration, "Electron reconstruction and identification at $\sqrt{s}$=7 TeV", *CMS Physics Analysis Summary* **CMS-PAS-EGM-10-004** (2010).

[21] CMS Collaboration, "Particle–Flow Event Reconstruction in CMS and Performance for Jets, Taus, and MET", *CMS Physics Analysis Summary* **CMS-PAS-PFT-09-001** (2009).

[22] CMS Collaboration, "Commissioning of the Particle-Flow Reconstruction in Minimum-Bias and Jet Events from pp Collisions at 7 TeV", *CMS Physics Analysis Summary* **CMS-PAS-PFT-10-002** (2010).

[23] M. Cacciari, G. Salam, and G. Soyez, "The anti-k_T jet clustering algorithm", *JHEP* **04** (2008) 063, doi:10.1088/1126-6708/2008/04/063.

[24] CMS Collaboration, "Jets in 0.9 and 2.36 TeV pp Collisions", *CMS Physics Analysis Summary* **CMS-PAS-JME-10-001** (2010).

[25] CMS Collaboration, "Determination of jet energy calibration and transverse momentum resolution in CMS", *Journal of Instrumentation* **6** (2011), no. 11, P11002.

[26] CMS Collaboration, "Identification of b-quark jets with the CMS experiment", *JINST* **8** (2013) P04013, doi:10.1088/1748-0221/8/04/P04013, arXiv:1211.4462.

[27] J. Alwall et al., "MADGRAPH 5 : Going Beyond", *JHEP* **1106** (2011) 128, doi:10.1007/JHEP06(2011)128, arXiv:1106.0522.

[28] P. Nadolsky et al., "Implications of CTEQ global analysis for collider observables", *Phys. Rev.* **D 78** (2008) 013004, doi:10.1103/PhysRevD.78.013004.

[29] T. Sjöstrand, S. Mrenna, and P. Skands, "PYTHIA 6.4 physics and manual", *JHEP* **05** (2006) 026, doi:10.1088/1126-6708/2006/05/026, arXiv:hep-ph/0603175.

[30] GEANT4 Collaboration, "GEANT4 – a simulation toolkit", *Nucl. Instr. and Methods A* **506** (2003) 250, doi:10.1016/S0168-9002(03)01368-8.

[31] J. M. Campbell and R. K. Ellis, "$t\bar{t}W^{\pm}$ production and decay at NLO", *JHEP* **07** (2012) 052, doi:10.1007/JHEP07(2012)052, arXiv:1204.5678.

[32] A. Kardos, Z. Trocsanyi, and C. Papadopoulos, "Top quark pair production in association with a Z-boson at NLO accuracy", *Phys. Rev. D* **85** (2012) 054015, doi:10.1103/PhysRevD.85.054015, arXiv:1111.0610.

[33] M. V. Garzelli et al., "Z^0-boson production in association with a $t\bar{t}$ pair at next-to-leading-order accuracy with parton shower effects", *Phys. Rev. D* **85** (2012) 074022, doi:10.1103/PhysRevD.85.074022, arXiv:1111.1444.

[34] J. Campbell, R. K. Ellis, and R. Röntsch, "Single top production in association with a Z boson at the LHC", arXiv:1302.3856.

[35] CMS Collaboration, "The fast simulation of the CMS detector at LHC", *J. Phys.: Conference Series* **331** (2011) 032049, doi:10.1088/1742-6596/331/3/032049.

[36] W. Beenakker et al., "Squark and gluino production at hadron colliders", *Nucl. Phys. B* **492** (1997) 51, doi:10.1016/S0550-3213(97)00084-9.

[37] A. Kulesza and L. Motyka, "Threshold resummation for squark-antisquark and gluino-pair production at the LHC", *Phys. Rev. Lett.* **102** (2009) 111802, doi:10.1103/PhysRevLett.102.111802.

[38] A. Kulesza and L. Motyka, "Soft gluon resummation for the production of gluino-gluino and squark-antisquark pairs at the LHC", *Phys. Rev. D* **80** (2009) 095004, doi:10.1103/PhysRevD.80.095004.

[39] W. Beenakker et al., "Soft-gluon resummation for squark and gluino hadroproduction", *J. High Energy Phys.* **12** (2009) 041, doi:10.1088/1126-6708/2009/12/041.

[40] W. Beenakker et al., "Squark and gluino hadroproduction", *Int. J. Mod. Phys. A* **26** (2011) 2637, doi:10.1142/S0217751X11053560.

[41] M. Kramer et al., "Supersymmetry production cross sections in pp collisions at $\sqrt{s} = 7$ TeV", arXiv:1206.2892.

[42] B. Knuteson and S. Mrenna, "BARD: Interpreting new frontier energy collider physics", arXiv:hep-ph/0602101.

[43] N. Arkani-Hamed et al., "MARMOSET: The Path from LHC Data to the New Standard Model via On-Shell Effective Theories", arXiv:hep-ph/0703088.

[44] J. Alwall, P. Schuster, and N. Toro, "Simplified Models for a First Characterization of New Physics at the LHC", *Phys. Rev. D* **79** (2009) 075020, doi:10.1103/PhysRevD.79.075020, arXiv:0810.3921.

[45] J. Alwall et al., "Model-Independent Jets plus Missing Energy Searches", *Phys. Rev. D* **79** (2009) 015005, doi:10.1103/PhysRevD.79.015005, arXiv:0809.3264.

[46] D. Alves et al., "Simplified Models for LHC New Physics Searches", arXiv:1105.2838.

[47] CMS Collaboration, "CMS Luminosity Based on Pixel Cluster Counting - Summer 2012 Update", *CMS Physics Analysis Summary* **CMS-PAS-LUM-12-001** (2012).

[48] T. Junk, "Confidence level computation for combining searches with small statistics", *Nucl. Instrum. Meth. A* **434** (1999) 435, doi:10.1016/S0168-9002(99)00498-2.

[49] A. L. Read, "Presentation of search results: The CL_s technique", *J. Phys. G* **28** (2002) 2693, doi:10.1088/0954-3899/28/10/313.

[50] ATLAS, CMS Collaboration, "Procedure for the LHC Higgs boson search combination in summer 2011", Technical Report ATL-PHYS-PUB-2011-011, CMS NOTE-2011/005, CERN, Geneva, (Aug, 2011).